Supporting Information

A Universal Strategy to Enhance Photothermal Conversion Efficiency by Regulating the Molecular Aggregation States for Safe Photothermal Therapy of Bacterial Infections

*Hao Fu, Yongxin Zhang, Cheng Wang, Zhencheng Sun, Shuyi Lv, Minghui Xiao, Kaiyu Wu, Linqi Shi, and Chunlei Zhu**

H. Fu, Y. Zhang, C. Wang, Z. Sun, S. Lv, M. Xiao, K. Wu, Prof. L. Shi, Prof. C. Zhu
Key Laboratory of Functional Polymer Materials of Ministry of Education, State Key Laboratory of Medicinal Chemical Biology, Tianjin Key Laboratory of Functional Polymer Materials, Frontiers Science Center for New Organic Matter, College of Chemistry
Nankai University
Tianjin 300071, China
Email: chunlei.zhu@nankai.edu.cn

Prof. C. Zhu
Beijing National Laboratory for Molecular Sciences
Beijing 100190, China

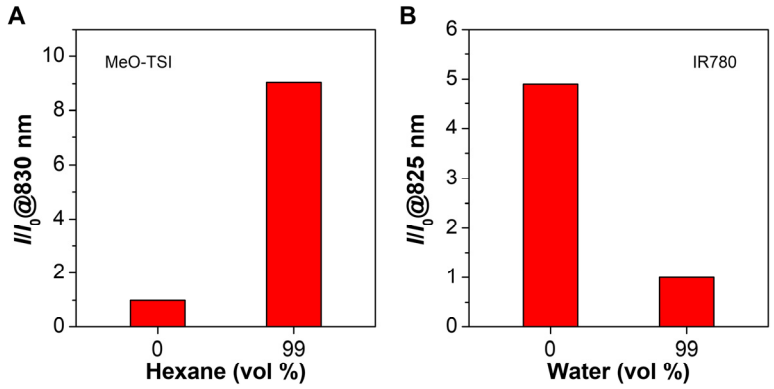

Figure S1. Relative emission intensity (I/I_0) of (A) MeO-TSI in hexane at 830 nm and (B) IR780 in water at 825 nm.

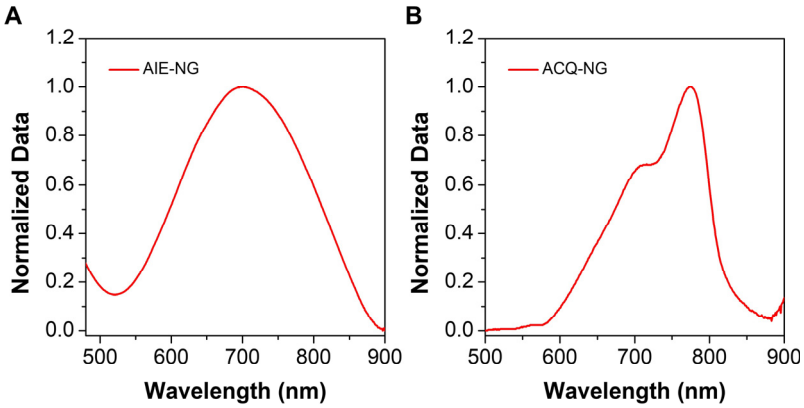

Figure S2. Normalized absorption spectra of (A) AIE-NG and (B) ACQ-NG.

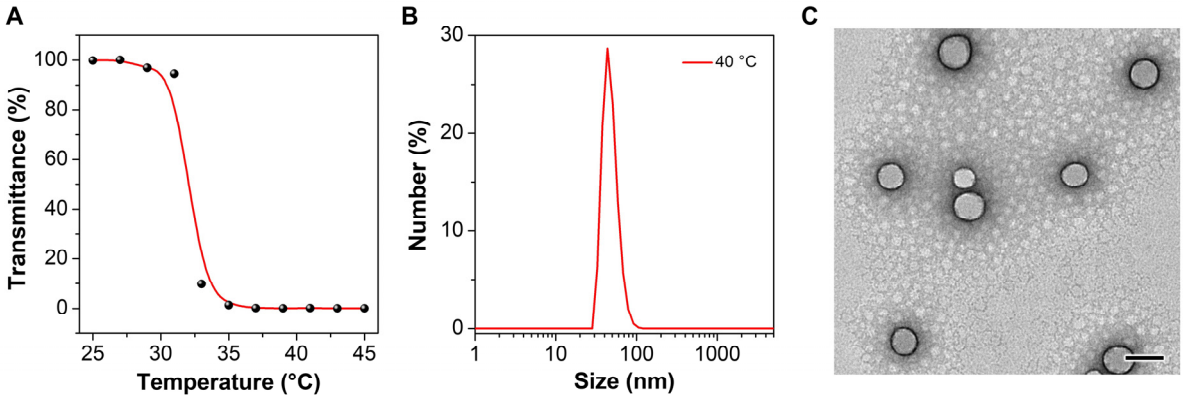

Figure S3. Characterizations on bare PNIPAM nanogels at different temperatures. A) Transmittance of bare PNIPAM nanogels at 808 nm as a function of temperature. B) Size distribution of bare PNIPAM nanogels at 40 °C measured by DLS. C) TEM image of bare PNIPAM nanogels. Scale bar: 100 nm.

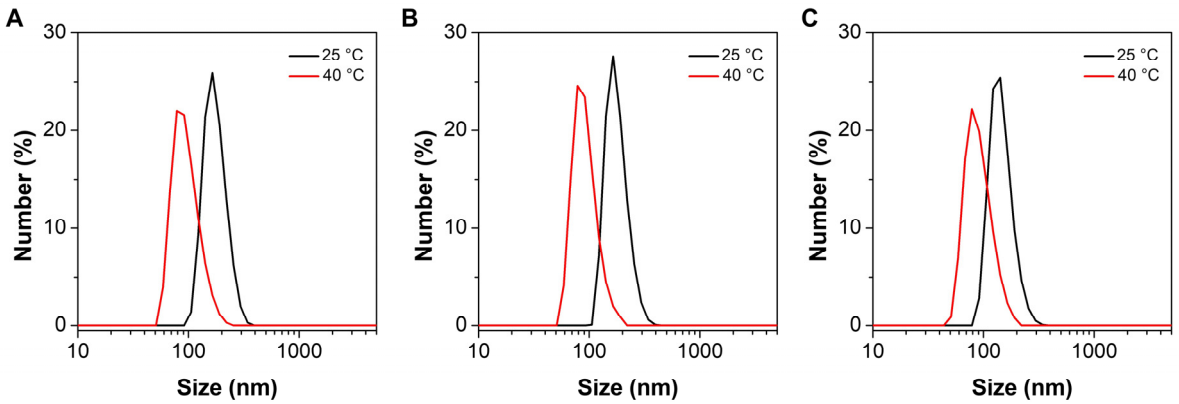

Figure S4. Size distribution of AIE-NG at 25 and 40 °C measured by DLS. A) LC = 1.47%. B) LC = 2.75%. C) LC = 4.26%.

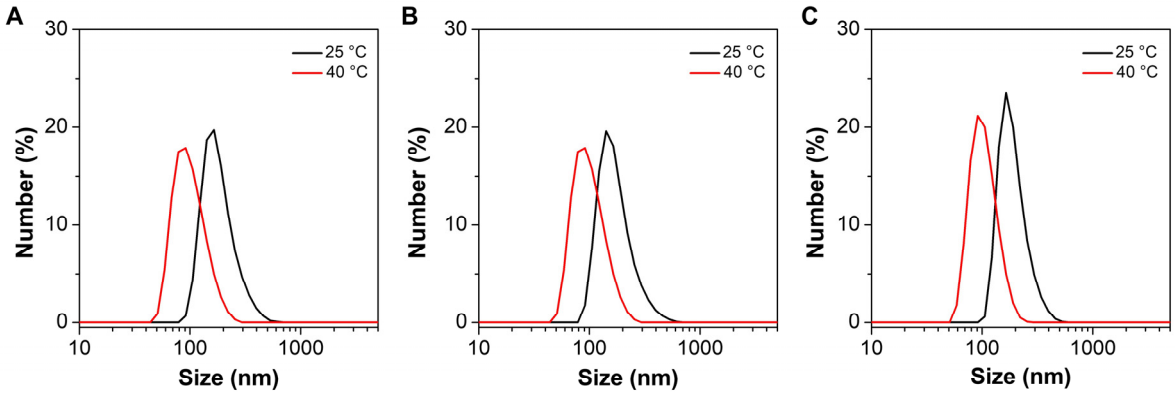

Figure S5. Size distribution of ACQ-NG at 25 and 40 °C measured by DLS. A) LC = 0.91%. B) LC = 1.65%. C) LC = 2.19%.

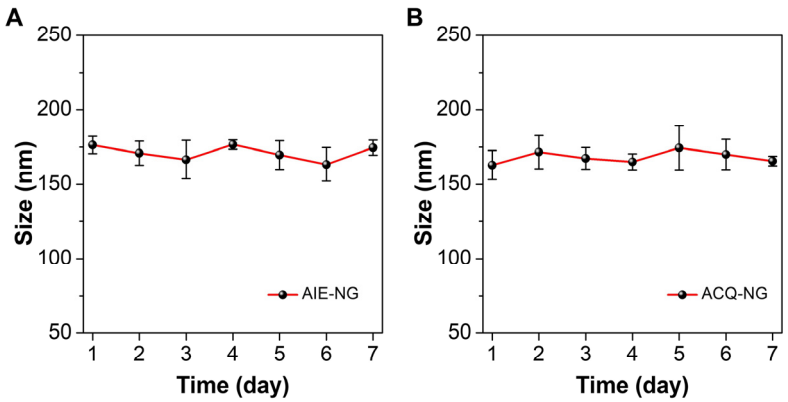

Figure S6. Particle size stability of (A) AIE-NG and (B) ACQ-NG at 25 °C during 7-day storage (n = 3).

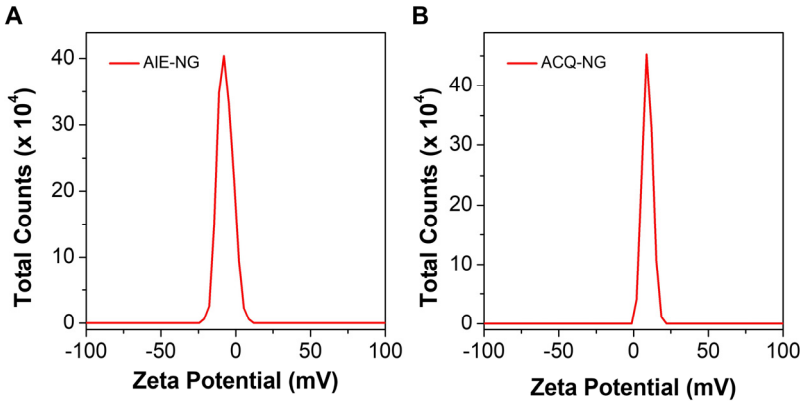

Figure S7. Zeta potentials of (A) AIE-NG and (B) ACQ-NG at 25 °C.

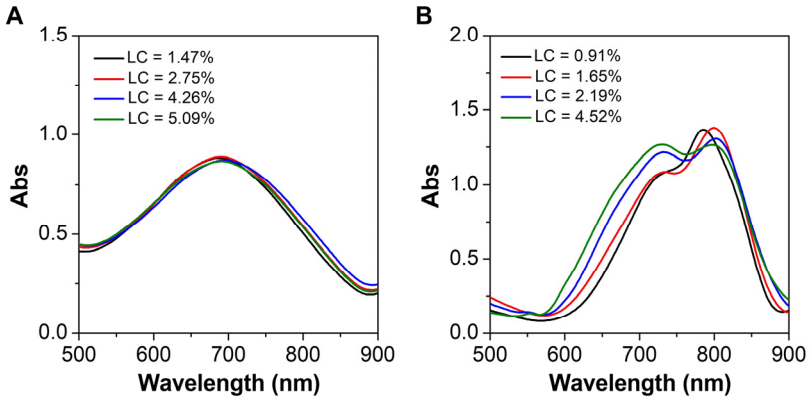

Figure S8. Absorption spectra of (A) AIE-NG (100 μM) and (B) ACQ-NG (100 μM) with different LC values.

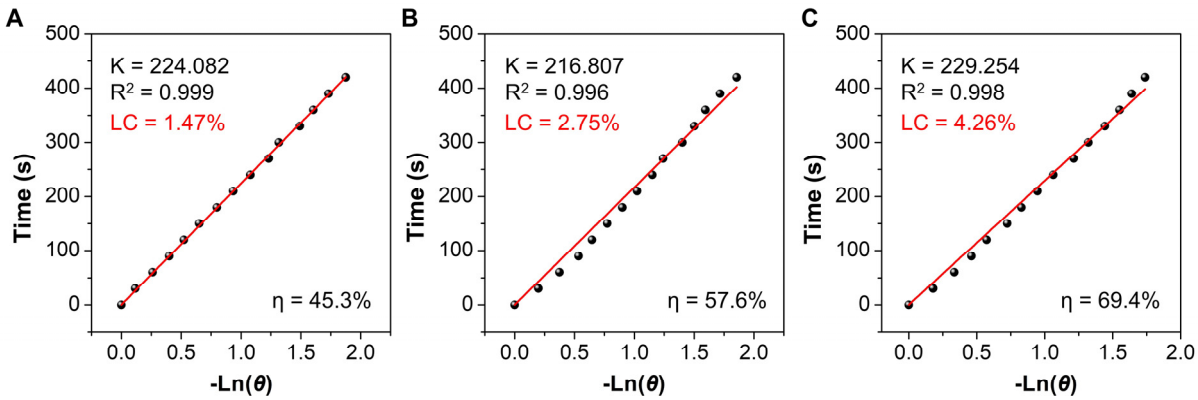

Figure S9. Linear fitting line of time as a function of -Ln θ obtained from the cooling curves of AIE-NG with different LC values. A) LC = 1.47%. B) LC = 2.75%. C) LC = 4.26%.

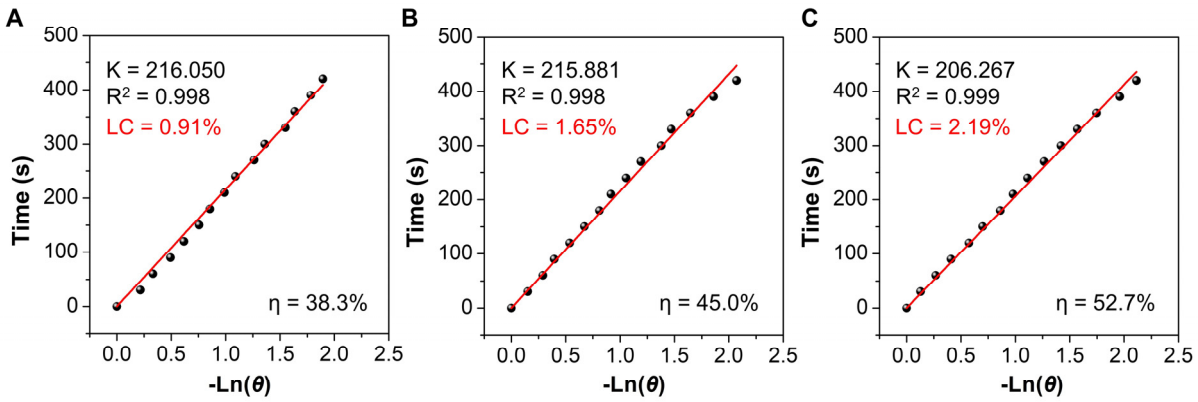

Figure S10. Linear fitting line of time as a function of -Ln θ obtained from the cooling curve of ACQ-NG with different LC values. A) LC = 0.91%. B) LC = 1.65%. C) LC = 2.19%.

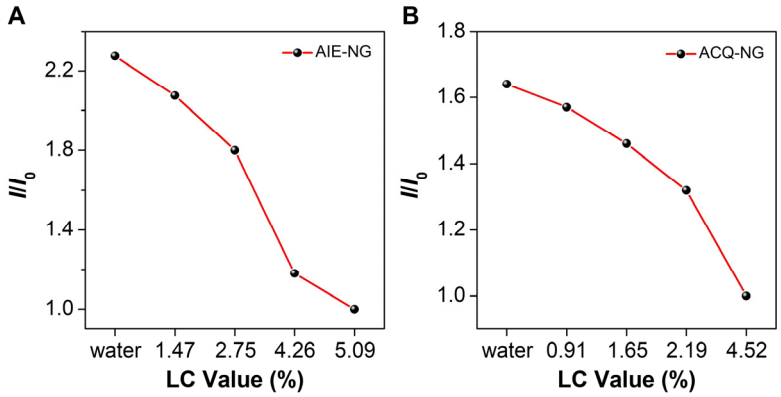

Figure S11. Relative emission intensity (I/I_0) at 525 nm of DCFH in the presence of (A) AIE-NG (100 μM) and (B) ACQ-NG (100 μM) with different LC values at 25 °C. I_0 denotes the emission intensity of AIE-NG (LC = 5.09%) or ACQ-NG (LC = 4.52%).

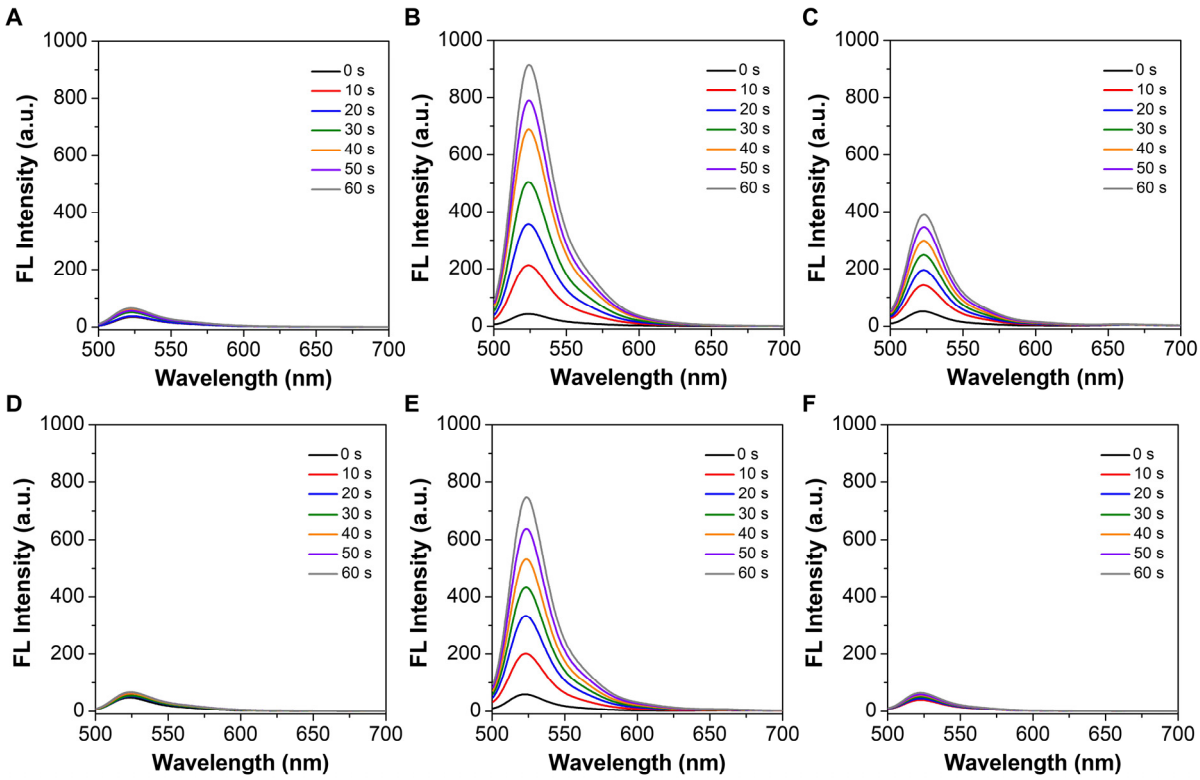

Figure S12. Emission spectra of DCFH in the presence of MeO-TSI self-aggregates (100 μM) and AIE-NG (LC = 5.09%, 100 μM) at different temperatures upon 808 nm NIR irradiation (0.3 W/cm^2). A) Blank at 25 °C. B) MeO-TSI self-aggregates at 25 °C. C) AIE-NG at 25 °C. D) Blank at 40 °C. E) MeO-TSI self-aggregates at 40 °C. F) AIE-NG at 40 °C.

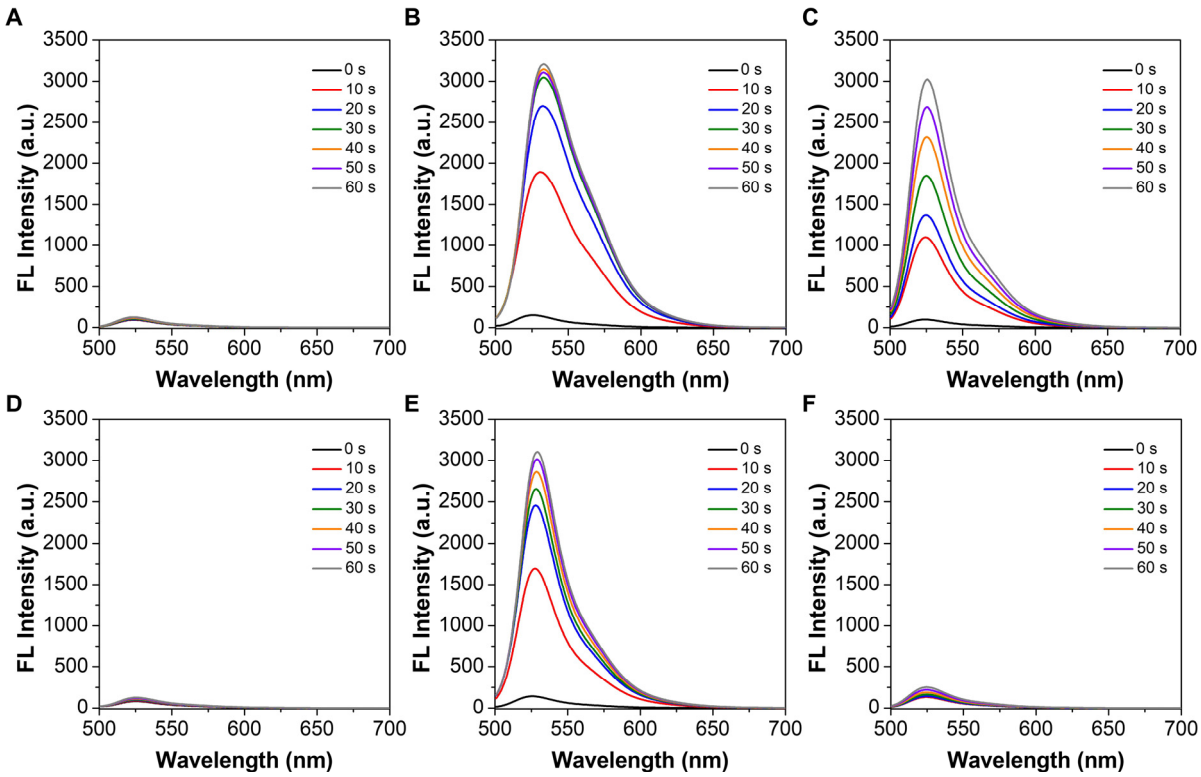

Figure S13. Emission spectra of DCFH in the presence of IR780 self-aggregates (100 μM) and ACQ-NG (LC = 5.09%, 100 μM) at different temperatures upon 808 nm NIR irradiation (0.3 W/cm^2). A) Blank at 25 °C. B) IR780 self-aggregates at 25 °C. C) ACQ-NG at 25 °C. D) Blank at 40 °C. E) IR780 self-aggregates at 40 °C. F) ACQ-NG at 40 °C.

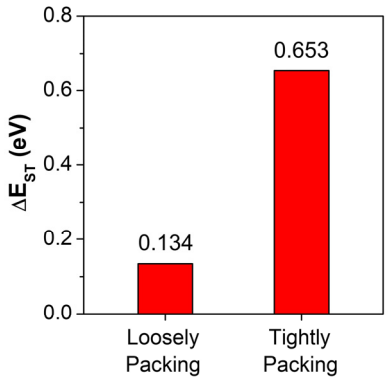

Figure S14. Calculated ΔE_{ST} between different singlet–triplet channels for loosely packed and tightly packed MeO-TSI.

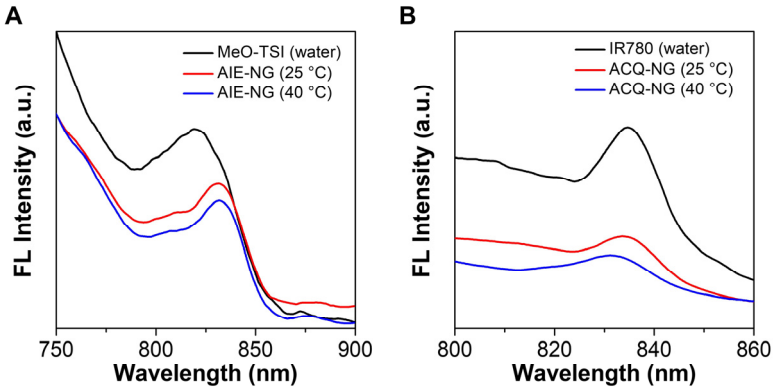

Figure S15. Emission spectra of (A) MeO-TSI (100 μM) and AIE-NG (LC = 5.09%, 100 μM) and (B) IR780 (100 μM) and ACQ-NG (LC = 4.52%, 100 μM) in water. Ex = 690 nm for MeO-TSI and AIE-NG; Ex = 780 nm for IR780 and ACQ-NG.

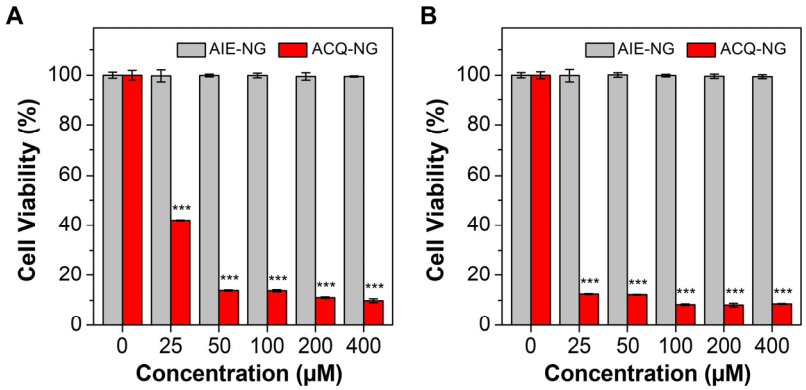

Figure S16. Viability of NIH-3T3 cells incubated with AIE-NG (LC = 5.09%) and ACQ-NG (LC = 4.52%) with varying concentrations for (A) 4 h and (B) 12 h, respectively (n = 3). ***p < 0.001 when compared with the blank group.

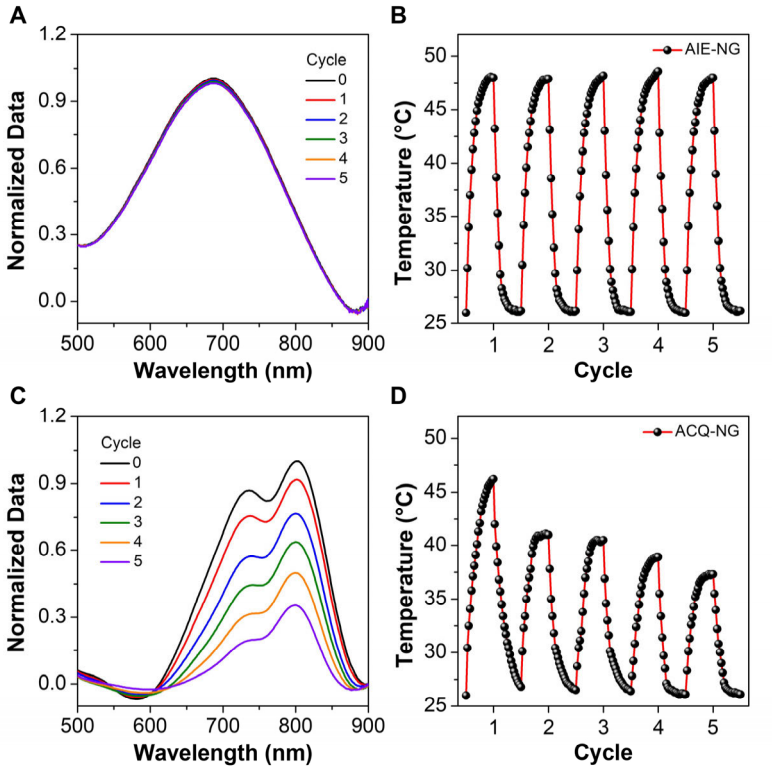

Figure S17. Photostability of AIE-NG (LC = 5.09%, 200 μM) and ACQ-NG (LC = 4.52%, 200 μM) upon repeated on-off irradiation with an 808 nm NIR irradiation (0.3 W/cm^2). A) Normalized absorption spectra of AIE-NG for five cycles of repeated on-off NIR irradiation. B) Temperature changes of AIE-NG for five cycles of repeated on-off NIR irradiation. C) Normalized absorption spectra of ACQ-NG for five cycles of repeated on-off NIR irradiation. D) Temperature changes of ACQ-NG for five cycles of repeated on-off NIR irradiation.

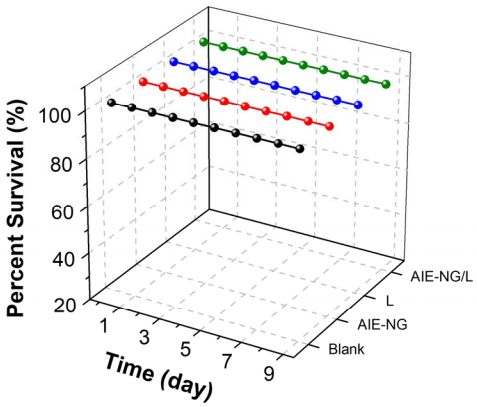

Figure S18. Survival rate of mice under different treatments as a function of time (n = 5).

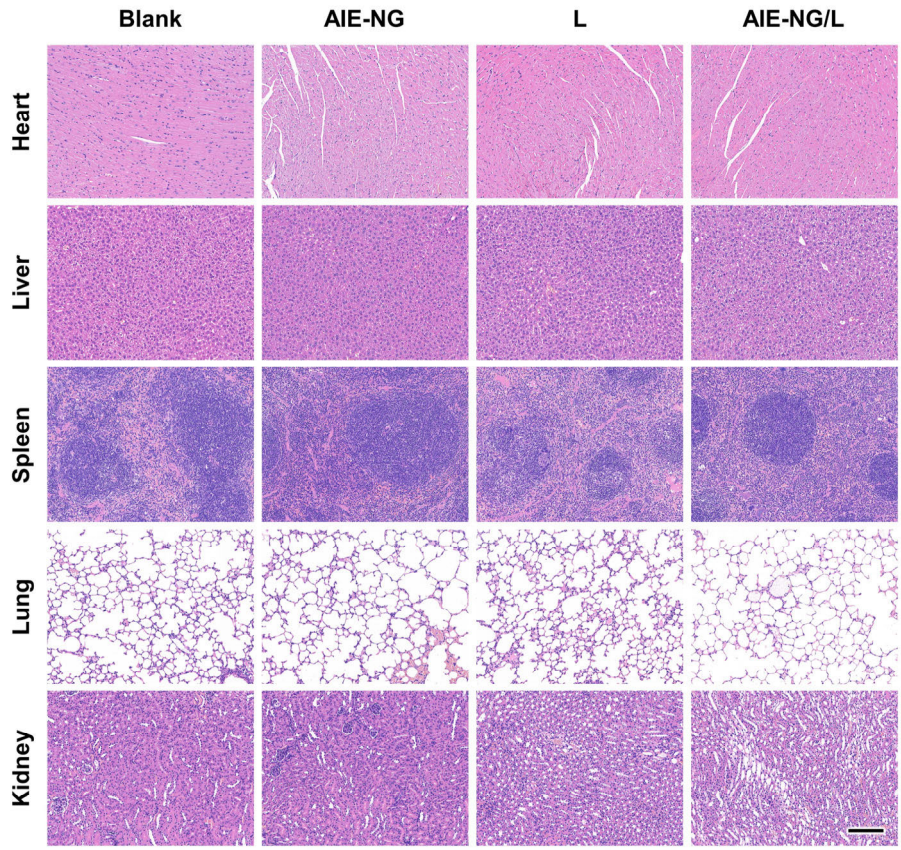

Figure S19. Histological analysis of different organs (heart, liver, spleen, lung, and kidney) from MRSA-infected mice stained by hematoxylin and eosin (H&E) on day 2. Scale bar: 50 μm.

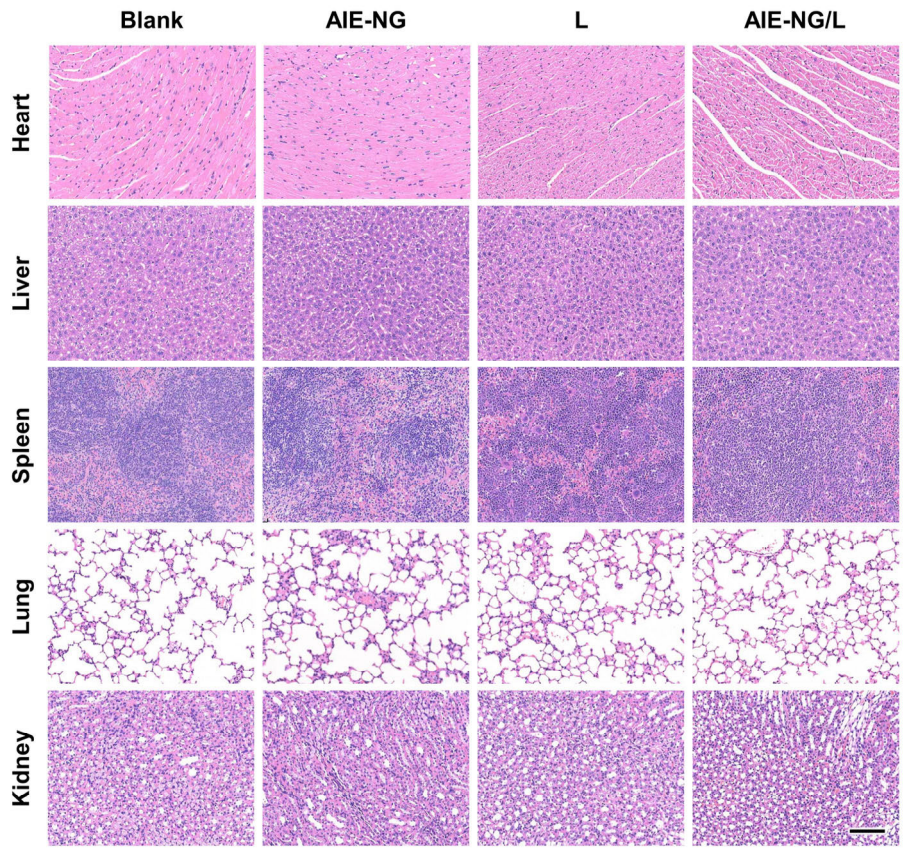

Figure S20. Histological analysis of different organs (heart, liver, spleen, lung, and kidney) from MRSA-infected mice stained by H&E on day 9. Scale bar: 50 μm.

Table S1. Calculations on the photothermal conversion efficiency of AIE-NG and ACQ-NG with varying LC values

	$\Delta T_{H_2O,\ surrounding}$ (°C)	$\Delta T_{max,\ surrounding}$ (°C)	$A_{808\ nm}$	τ (s)	hS (W/°C)	η
MeO-TSI self-aggregates	0.4	11.1	0.504	217.142	0.00967	41.7%
LC = 1.47%	0.4	12.7	0.486	224.082	0.00937	45.3%
LC = 2.75%	0.4	13.5	0.507	216.807	0.00969	57.6%
LC = 4.26%	0.4	16.5	0.539	229.254	0.00916	69.4%
LC = 5.09%	0.4	18.0	0.498	223.109	0.00941	80.9%
IR780 self-aggregates	0.2	7.6	0.792	194.681	0.01079	31.6%
LC = 0.91%	0.2	9.1	1.205	216.050	0.00972	38.3%
LC = 1.65%	0.2	11.6	1.351	215.881	0.00973	45.0%
LC = 2.19%	0.2	13.1	1.295	206.267	0.01018	52.7%
LC = 4.52%	0.2	14.7	1.242	204.217	0.01028	64.4%